



## Front-end design at 22 GHz for the Gregorian focus of the new Sardinia Radio Telescope

L. Cresci<sup>1</sup>, L. Lucci<sup>2</sup>, A. Orfei<sup>3</sup>, V. Natale<sup>1</sup>, R. Nesti<sup>1</sup>, D. Panella<sup>1</sup>,  
G. Pelosi<sup>2</sup>, and L. Rossi<sup>2</sup>

<sup>1</sup> INAF - Istituto di Radioastronomia, Sez. di Firenze, Largo E. Fermi 5, I-50125 Firenze

<sup>2</sup> Università di Firenze, Dip. di Electronica e Telecomunicazioni, Via Lombroso 6/17, I-50125 Firenze

<sup>3</sup> INAF - Istituto di Radioastronomia, Via P. Gobetti 101, I-40129 Bologna

**Abstract.** In this contribution the design of the front-end of the 22-GHz cooled receiver for the Sardinia Radio Telescope (SRT) is presented. It comprises a corrugated horn feed, a directional coupler and a polarizer. A quite original design approach has been adopted since these devices have been optimized for high performance in the 19–26 GHz-band. Prototypes of the above components have been produced and tested highlighting very good agreement with the expected electromagnetic behaviour. Furthermore, in this contribution the effects of the beam in the sky due to the above front-end feeding the Gregorian dual-mirror configuration of the SRT are analyzed.

### 1. Introduction

The development of the SRT receivers is one of the main technological challenges involving people dealing with radio astronomical instrumentation.

In particular, in these very early times of the radio telescope being constructed, the 22-GHz passive front-end is of relevant interest since it has to show high performance over a broad (33%) frequency band operating in circular polarization. Furthermore a 7-element focal plane array is considered for the Gregorian focus of the antenna, implying extra effort and care in the design, with respect to the single-element case.

Three devices are discussed here: the corrugated feed horn, the coupler and the po-

larizer. The feed model is not of standard type (Olver et al. 1994), since critical issues of space constrain to adopt curved corrugation profiles, optimized for horn compactness (Gentili et al. 2000). Also for the polarizer and the coupler, solutions quite far from common devices (e.g. Uher et al. 1993) have been considered. The polarizer is composed by a Differential Phase Shifter (DPS), followed by an Orthomode Transducer (OMT), while the coupler is developed in circular waveguide, constituting the main branch, with the coupled port being in standard WR42 rectangular waveguide. The effects of the beam in the sky due to the feed coupling with the antenna mirrors are considered. For this purpose the *Grasp* 8 software package has been used. Finally the efficiency, the antenna temperature and the  $G/T$  factor are discussed.

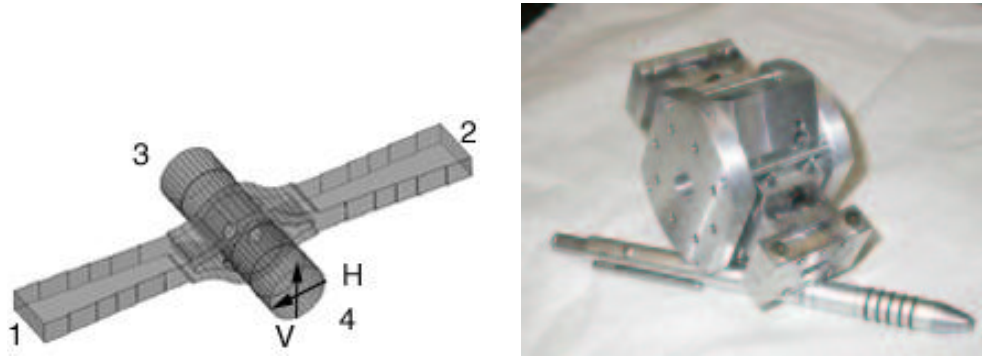


**Fig. 1.** CWC: electromagnetic model (a) and prototype (b).

## 2. Circular waveguide coupler

The task of the coupler is to add calibration and service signals into the receiver chain. There are two main reasons for the use of a coupler straight after the feed: the first one is the possibility of calibrating most of the receiver devices (the feed is the only one excluded); the second one is a 50% reduction in the number of couplers and, consequently, in the number of cables feeding them. In fact, by using standard rectangular waveguide couplers, the polarizer calibration is not feasible and, since the polarizer doubles the waveguide channels, in this particular case of a 7-element receiver array the total number of couplers should be 14 instead of 7.

The main drawback of the circular coupler, with respect to the rectangular one, is the worse coupling performance. Furthermore, in applications like this one, where the cross-talk between the two polarizations needs to be very low, the device must be carefully designed, since the azimuth asymmetry of circular coupler configurations, necessary for proper operation, does contribute to the depolarization of the signal in the main branch. This problem does not occur in the rectangular coupler since it is placed after polarization splitting (produced by the polarizer) and the main branch propagates only one mode.

The circular waveguide coupler (CWC) design led to the electromagnetic model in Fig. 1a. It is a 4-physical port device: two in rectangular waveguide (1, 2) and two in circu-

lar waveguide (3, 4). To each circular waveguide port two modes are associated representing the **H** and **V** polarization states of the  $TE_{11}$  fundamental mode of propagation.

A prototype of the CWC is shown in Fig. 1b and its measured performance is given in Fig. 2. The plots in Fig. 2a are related to the scattering parameters between the coupled rectangular waveguide and the main circular waveguide branch. The reflection coefficient ( $S_{11}$ ) shows good performance, being below  $-22$  dB in almost all of the bandwidth. The rectangular waveguide is uncoupled, by symmetry, from the **H** polarization and the related scattering parameters are not plotted. Instead port 1 is coupled to the **V** polarization of port 4 and the coupling coefficient is given by the  $S_{14V}$  curve. The directional properties of the coupler can be seen by comparing this curve with the isolation one indicated as  $S_{13V}$  and representing the coupling between port 1 and the **V** polarization of port 3.

Although the coupling and isolation curves are not as flat as in the case of the standard rectangular waveguide coupler, they are however reasonably acceptable.

The other plot (Fig. 2b) is related to the main branch of the CWC, particularly to those effects which can alter the receiver performance. The reflection coefficient seen at port 3 for the two polarizations are associated to the  $S_{33H}$  and  $S_{33V}$  curves and values need to be read on the left ordinate axis. They are very low (below  $-30$  dB in almost all of the band-

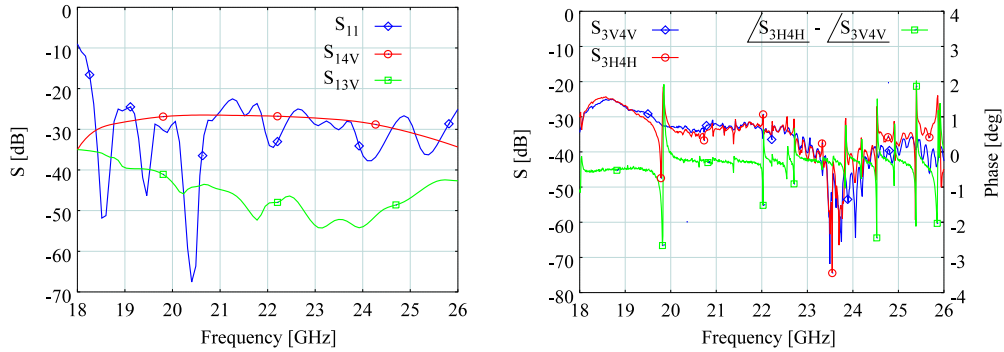


**Fig. 2.** CWC scattering parameters: (a) rectangular to circular coupling; (b) main branch.

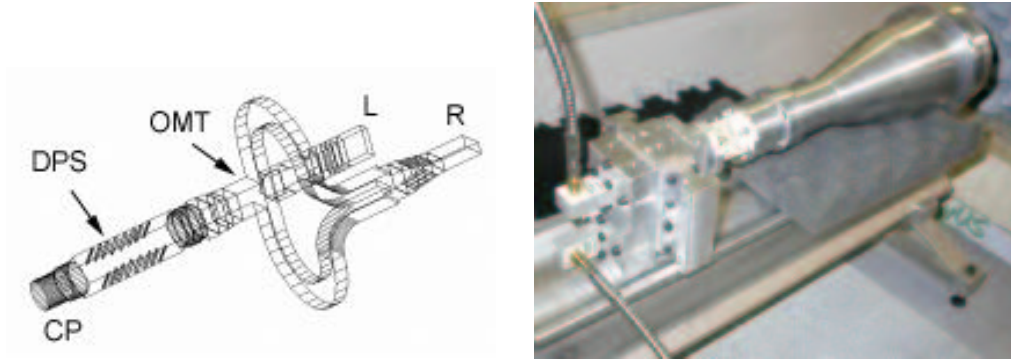


**Fig. 3.** Polarizer: electromagnetic model (a) and prototype (b).

width) and very similar to each other, although some spikes should be noted in the  $\mathbf{H}$  polarized signal. This similarity is confirmed by the differential phase shift curve (the difference in the phase between the  $S_{34H}$  and the  $S_{34V}$  scattering parameters) which shows the same spike frequencies of  $S_{33H}$ . The amplitude and phase equality between  $S_{34H}$  and  $S_{34V}$  is very important to prevent signal depolarization. Let's consider the differential phase shift curve on the right ordinate axis of Fig. 2b (the dominant factor for cross-talk degradation once the spikes are eliminated): measurement data highlight a mean value of about  $0.3^\circ$ , corresponding to a very good cross-talk upper limit of about  $-50$  dB.

Although the general behavior is quite good, for acceptable performance the spikes, almost certainly due to fabrication imperfec-

tions, need to be removed. This aspect is still under investigation.

### 3. Polarizer

The polarizer is a 3-physical-port device and, from a receiver point of view, it has one input port (*Common Port* [CP]) and two output ports, the *Left Port* (L) and the *Right Port* (R). At the CP a dual circularly polarized signal (*Left Hand Circular Polarization* [LHCP] and *Right Hand Circular Polarization* [RHCP]) is fed from the horn and the polarizer separates these polarizations into two waveguides, the LHCP in the L-port and the RHCP in the R-port. The electromagnetic model of the polarizer is given in Fig. 3a and the prototype is shown in Fig. 3b in the test setup (loaded with a corrugated horn).

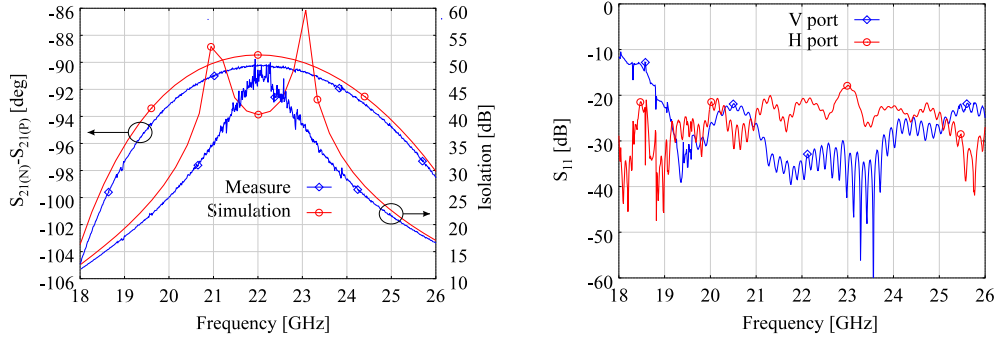


**Fig. 4.** Polarizer performance: DPS phase shift and cross-talk (a) and reflection (b).

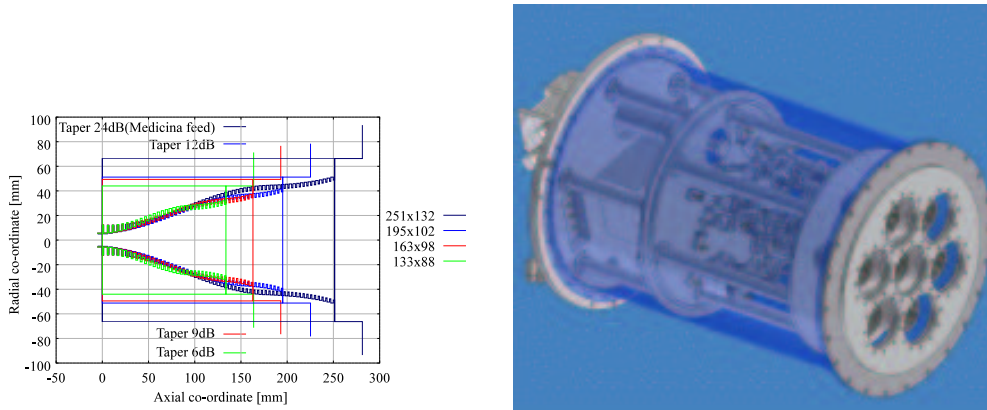


**Fig. 5.** Geometrical comparison among different feeds (a) and array receiver inside the dewar (b).

This design is quite broadband as can be seen by the plots in Fig. 4. The circular-to-linear polarization transformation features are given by the DPS, whose performance is shown in Fig. 4a, reporting the comparison between simulation and measurement of the differential phase shift and the cross-talk. Analogously to the circular coupler previously discussed, the DPS differential phase shift is defined between scattering parameters associated to two linear polarizations: in this case the first ( $S_{21(N)}$ ) is normal and the second ( $S_{21(P)}$ ) parallel to the irises. The shift, given by the bell-like curves (readable on the left ordinate scale), should be  $-90^\circ$ , but it is impossible to obtain a precisely flat curve in the band

of interest. The best feasible performance is to have a parabolic shape, as flat as possible in the vertex and centered in the bandwidth, crossing the ideal  $-90^\circ$  curve in two points (double zero design). Since the DPS return loss is very high (above 30 dB, not shown), the DPS cross-talk is essentially determined by the differential phase shift curve and it is shown in the same Fig. 4a, with related values reported on the right ordinate scale. Assuming an ideal behavior of the OMT that follows the DPS, this performance degradation parameter physically represents the ratio between the power signals out from the R(L) and the L(R) port of the polarizer, when the input is a LHCP (RHCP) waveform at the CP port. In this particular design we are required to have a very low cross-

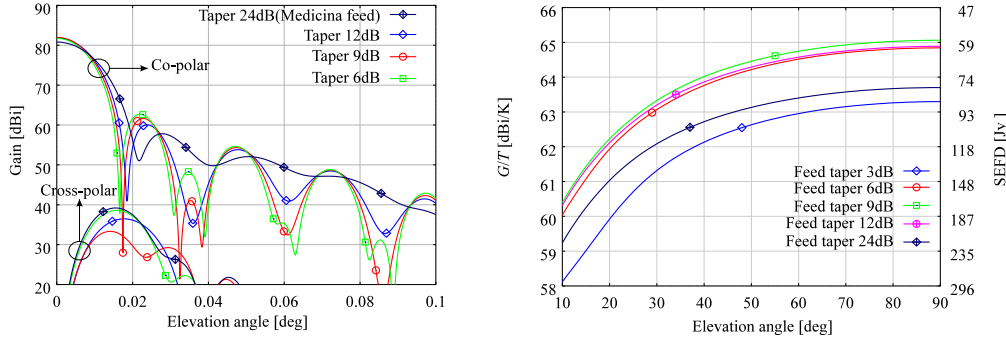


**Fig. 6.** Performance comparison: ‘beam in the sky’ (a) and  $G/T$  (SEFD) (b).

talk ( $< -35$  dB according to VLBI<sup>1</sup> requirements) in a small frequency sub-band around 22 GHz. The OMT is based on the Bøifot junction (Bøifot et al. 1990), guaranteeing broadband and high performance separations in two waveguides of the linear polarizations out from the DPS.

In the test setup of Fig. 3b, the reflection coefficients at the R and L port of the polarizer were measured, showing very high performances, with curves below  $-20$  dB in almost the whole 18–26 GHz-wide band (see Fig. 4b).

#### 4. Feed design and antenna performance

Corrugated feeds have been studied to optimize the efficiency of the SRT Gregorian configuration. The secondary ellipsoidal mirror has an interfocal distance of about 17.6476 m and a diameter of 7.9060 m, leading to an edge angle<sup>2</sup> of about  $12^\circ$ .

The tapering level at this angle has been used as a parameter to evaluate the performance of different feeds, designed to optimize electrical (maximizing the efficiency) and mechanical (minimizing the space occupation) aspects. In Fig. 5a the corrugation profile of different corrugated feed horns, providing distinctive tapering, is shown. The space occupation

associated to each feed is put in evidence by boxing each profile and it is important to notice that by decreasing the taper the feed volume decreases as well. As can be read on the right-hand side of Fig. 5a, a very strong taper of 24 dB requires a feed of about 251 mm length and 132-mm aperture diameter, while a 6-dB taper feed needs a cross-section area of about  $133 \text{ mm} \times 88 \text{ mm}$ .

Since the single feed is part of a 7-element array receiver, to be cooled at 20 K inside a dewar, as shown in the drawing in Fig. 5b, the importance of reducing feed volume and weight becomes clear.

The performance of each feed is evaluated as part of the optical system. In Fig. 6a the  $45^\circ$ -cut pattern (co-polar and cross-polar components) of the SRT Gregorian configuration antenna fed by different horns is shown. The plots highlight a HPBW<sup>3</sup> around  $0^\circ 006$ , cross-polarization down  $-40$  dB and side lobes below  $-20$  dB (the side lobe level decreases as the taper increases). The gain-over-system temperature ( $G/T$ ) is given as a function of the elevation angle on the left ordinate scale of Fig. 6b, with corresponding values of the SEFD<sup>4</sup> given in Jansky<sup>5</sup> [Jy] on the right ordinate scale. From the  $G/T$  curves and the data

<sup>3</sup> Half Power Beam Width

<sup>4</sup> System Equivalent Flux Density.  $SEFD = \frac{8\pi k}{G/T} \left(\frac{L}{c}\right)^2$ , where  $f$  is the frequency,  $k = 1.38 \times 10^{-23} \text{ JK}^{-1}$  is the Boltzmann constant and  $c = 3 \times 10^8 \text{ ms}^{-1}$  is the light speed in vacuum

<sup>5</sup>  $1 \text{ Jy} = 10^{-26} \text{ Wm}^{-2}\text{Hz}^{-1}$

<sup>1</sup> Very Large Baseline Interferometry

<sup>2</sup> The angle at which a geometrical ray coming from the feed position intercepts the edge of the reflector

**Table 1.** Feed performance comparison at 22 GHz. The efficiency includes illumination and spillover

Taper@12°[dB]	Volume [dm <sup>3</sup> ]	Gain [dBi]	Efficiency [%]	$G/T@10^\circ$ [dBi/K]	$G/T@90^\circ$ [dBi/K]
3	-	-	-	58.12	63.30
6	0.27	81.72	68.39	60.04	64.84
9	0.41	81.98	72.61	60.40	65.06
12	0.53	81.87	70.69	60.31	64.89
24	1.14	80.81	55.46	59.23	63.70

summarized in Table 1 we conclude that the 9 dB taper feed optimizes the space occupation with the best electrical performance.

## References

- Bøifot, A.M., Lier, E., & Shaug-Pettersen, T. 1990, IEE Proc. H, Vol. 137-6, p. 396
- Gentili, G.G, Nesti, R., Pelosi, G., & Natale, V. 2000, Electronics Letters, 36, No. 6, p. 486
- Olver, A.D., Clarricoats, P.J.B., Kishk, A.A., & Shafai, L. 1994, Microwave Horns and Feeds (IEE, London)
- Uher, J., Bornemann, J., & Rosenberg, U. 1993, Waveguide Components for Antenna Feed System: Theory and CAD (Artech House, London)